

Soliton collision, modulation instability and long-time asymptotic for non-autonomous solutions in the variable-coefficient coupled Schrödinger-KdV equations

Tongshan Liu(刘桐杉), Li Li(李丽), Fajun Yu(于发军)
Citation: Chin. Phys. B. 35, 090201 (2026). DOI: 10.1088/1674-1056/ae60ed |
CSTR: 32038.14.CPB.ae60ed
http://cpb.iphy.ac.cn; http://iopscience.iop.org/cpb

What follows is a list of articles you may be interested in

Degenerate solitons and asymptotic analysis for a three-coupled fourth-order nonlinear Schrödinger system in an alpha helical protein

Dan-Yu Yang(杨丹玉)
Chin. Phys. B. 35, 020201 (2026). DOI: 10.1088/1674-1056/adf4a5 | CSTR: 32038.14.CPB.adf4a5

Dynamical analysis and localized waves of the n-component nonlinear Schrödinger equation with higher-order effects

Yu Lou(娄瑜), Guoan Xu(许国安)
Chin. Phys. B. 34, 030201 (2025). DOI: 10.1088/1674-1056/ada435 | CSTR: 32038.14.CPB.ada435

Soliton propagation for a coupled Schrödinger equation describing Rossby waves

Li-Yang Xu(徐丽阳), Xiao-Jun Yin(尹晓军), Na Cao(曹娜), Shu-Ting Bai(白淑婷)
Chin. Phys. B. 32, 070202 (2023). DOI: 10.1088/1674-1056/acb9e5

Multi-symplectic method for the coupled Schrödinger-KdV equations

Zhang Hong(张弘), Song Song-He(宋松和), Zhou Wei-En(周炜恩), Chen Xu-Dong(陈绪栋)
Chin. Phys. B. 23, 080204 (2014). DOI: 10.1088/1674-1056/23/8/080204

Average vector field methods for the coupled Schrödinger–KdV equations

Zhang Hong(张弘), Song Song-He(宋松和), Chen Xu-Dong(陈绪栋), Zhou Wei-En(周炜恩)
Chin. Phys. B. 23, 070208 (2014). DOI: 10.1088/1674-1056/23/7/070208

SPECIAL TOPIC — Nonlinear localized waves: Theory, methods and applications

Soliton collision, modulation instability and long-time asymptotic for non-autonomous solutions in the variable-coefficient coupled Schrödinger-KdV equations

Tongshan Liu(刘桐杉), Li Li(李丽), and Fajun Yu(于发军)†

School of Mathematics and Systematic Sciences, Shenyang Normal University, Shenyang 110034, China

(Received 31 January 2026; revised manuscript received 25 March 2026; accepted manuscript online 17 April 2026)

This paper extends the coupled Schrödinger-KdV equations by incorporating variable time-dependent coefficients. The Hirota bilinear method is employed to systematically derive the bilinear form of the variable-coefficient coupled Schrödinger-KdV equations. Explicit expressions for non-autonomous one- and two-soliton solutions are obtained with time-dependent variations in amplitude, width, and velocity. The principal advantage of the variable-coefficient model lies in its ability to achieve precise theoretical control over soliton generation, transmission, shaping, and interactions through appropriate design of the time-evolution of coefficient functions such as $a(t)$ and $b(t)$. Then, the asymptotic behaviors of the two-soliton solutions are analyzed in two distinct cases. Moreover, modulational instability is also investigated, demonstrating how small perturbations can grow under variable-coefficient conditions, which is crucial for evaluating soliton stability. This controllability indicates potential applications in optical communication systems.

Keywords: coupled Schrödinger-KdV equations, Hirota bilinear method, soliton collision, long-time asymptotic

PACS: 02.20.Sv, 02.30.Ik, 02.30.Jr

DOI: 10.1088/1674-1056/ae60ed **CSTR:** 32038.14.CPB.ae60ed

1. Introduction

The nonlinear Schrödinger equation (NLSE) is regarded as a fundamental model in modern mathematical physics, as it can be systematically derived from first principles under the slowly varying envelope approximation. It captures the essential interplay between dispersion and nonlinearity, which governs wave propagation in a wide range of physical systems, including nonlinear optics, plasma physics, and Bose–Einstein condensates.[1] Historically, the NLSE was first introduced to describe the evolution of slowly varying wave envelopes in weakly nonlinear and dispersive media. In nonlinear optics, it arises naturally from Maxwell's equations under the paraxial and slowly varying envelope approximations, where the Kerr nonlinearity plays a central role. Its standard form successfully characterizes the self-phase modulation and stable transmission of envelope solitons, finding widespread applications in nonlinear optics and plasma physics.[2–4] However, despite its remarkable success, the standard NLSE is based on the assumption of constant coefficients, which limits its applicability in realistic physical environments. In many practical situations, such as optical fibers with varying dispersion or nonlinear media with spatial inhomogeneity, the system parameters evolve with time or space. Consequently, the variable coefficient nonlinear Schrödinger equation (VC-NLSE) was proposed to incorporate time-dependent coefficients, providing a more realistic and flexible framework for modeling nonlinear wave propagation.[5] This generalized model enhances the precision of physical simulations and offers possibilities for active soliton control, including compression, amplification, and collision management.[6,7] It exhibits a richer mathematical structure and broader application scope. For instance, it is used to simulate wave propagation in inhomogeneous media,[6] such as those involving constrained Lax pairs and conservation laws.

Solving variable-coefficient nonlinear equations and analyzing their dynamical properties pose far greater challenges than those encountered in constant-coefficient models. Traditional methods, such as the inverse scattering transform, are often difficult to apply directly, thus prompting scholars to develop powerful and effective analytical tools. In this research field, the Hirota bilinear method stands out in Refs. [3,8–10]. It transforms the original nonlinear equation into a set of bilinear forms through clever variable transformations (such as $u = g/f$), and then systematically constructs multi-soliton solutions through formal power series expansions. The advantage of this method lies in its algebraic operations and direct construction. It has been successfully applied to a series of integrable systems, ranging from the KdV equation[11] to the constant coefficient NLSE. Yang–Ma's research shows that under specific coefficient constraints, the variable-coefficient NLSE

†Corresponding author. E-mail: yufajun888@163.com

© 2026 Chinese Physical Society and IOP Publishing Ltd. All rights, including for text and data mining, AI training, and similar technologies, are reserved.

can also be accurately bilinearized.[12] Using this method, Wang–Zhang–Yang successfully derived the non-autonomous soliton solutions for the variable-coefficient model and observed a wealth of interaction phenomena, including elastic collisions, periodic evolution, parabolic trajectories, as well as novel "S-shaped" and "π-shaped" soliton structures.[13] These results lay a solid foundation for understanding the robustness and controllability of solitons in complex environments.[14]

In recent years, nonlinear evolution equations with variable coefficients have attracted considerable attention, mainly due to their capability to describe nonlinear wave propagation in realistic, inhomogeneous, and nonuniform media. Compared with constant-coefficient models, such systems allow dispersion and nonlinear effects to vary with time and space, which leads to richer wave structures and more flexible dynamical behaviors. Consequently, significant efforts have been devoted to constructing exact solutions and investigating nonlinear wave dynamics in variable-coefficient models. Notable advances include the application of symmetry reduction approaches to nonlinear evolution equations, through which exact solutions such as Painlevé-type solitons can be constructed.[15] The phase structures and topological properties of rogue waves have been investigated through the concept of virtual Dirac monopoles, providing new insights into nonlinear wave phenomena.[16] Furthermore, soliton interactions and collision dynamics in variable-coefficient coupled nonlocal nonlinear Schrödinger systems have been systematically studied, showing that system parameters can significantly influence the dynamical behaviors of nonlinear waves.[17] In addition, vortex solitons in atomic-molecular Bose–Einstein condensates with optical lattice potentials have been reported, revealing complex nonlinear wave structures in Bose–Einstein condensate systems.[18] Explicit soliton solutions and blow-up phenomena for such coupled equations have also been investigated, exhibiting rich dynamical behaviors in non-autonomous nonlinear systems.[19] Moreover, the Hirota bilinear method has been successfully applied to construct multiple-soliton solutions for variable-coefficient KdV-type equations, while various soliton structures for nonlinear Schrödinger-type equations have been derived through Hirota transformations.[20] More complex nonlinear wave structures, including lump and rogue-wave solutions, have also been obtained for related nonlinear systems. These studies collectively demonstrate that the Hirota bilinear method serves as a powerful analytical tool for deriving exact solutions and understanding nonlinear wave dynamics in variable-coefficient nonlinear systems.

A significant distinction arises when comparing the variable-coefficient model considered in this work with the classical constant-coefficient Schrödinger-KdV system. The variable-coefficient framework provides a more realistic description of nonlinear wave propagation in many physical environments. In numerous real-world systems — such as dispersion-managed optical fibers, plasmas with nonuniform density, and fluid systems under external forcing — the governing parameters naturally depend on time or spatial variables.[6,21] These spatiotemporal variations can strongly influence the amplitude, velocity, and localization characteristics of nonlinear waves. In constant-coefficient systems, soliton propagation typically occurs with fixed velocity and invariant wave shape. By contrast, the introduction of variable coefficients leads to time-dependent modulation of soliton propagation, enabling more complex dynamical behaviors.[6,21] Consequently, the propagation speed, amplitude evolution, and localization properties of nonlinear waves can be effectively controlled through variable coefficients.

Therefore, investigating the analytical solutions and dynamical properties of variable-coefficient nonlinear systems is of great importance for understanding controllable nonlinear wave phenomena in inhomogeneous media.

The original coupled Schrödinger-KdV (CS-KdV) equation has been augmented with variable coefficients as follows:

$$\begin{aligned} &q_t(x,t)-a(t)q_{xx}(x,t)-b(t)q(x,t)w(x,t)=0,\\ &w_t(x,t)+c(t)w(x,t)w_x(x,t)+d(t)w_{xxx}(x,t)\\ &-l^2(t)(|q_x(x,t)|^2)=0, \end{aligned} \tag{1}$$

here, $a(t)$, $b(t)$, $c(t)$, $d(t)$, $l(t)$ are time-dependent coefficient functions that can simulate the evolution of physical system environments, such as external field modulation or slow changes in medium properties. This model generalizes the standard case to investigate soliton dynamics in more complex settings,[12] including inhomogeneous plasmas.[22]

In this work, we focus on a variable-coefficient coupled Schrödinger-KdV (CS-KdV) equation, which serves as an effective model for describing nonlinear wave interactions in non-uniform media. Exact soliton solutions are constructed using the Hirota bilinear method, and the interaction properties of solitons are analyzed in detail. In addition, the modulational instability (MI) of the system is investigated, revealing how variable coefficients influence soliton stability and robustness. These results provide useful insights into the controllability of soliton dynamics in complex physical environments. The remainder of this paper is organized as follows. In Section 2, the variable-coefficient CS-KdV equation is bilinearized via appropriate variable transformations, and the one-soliton solution is derived. Section 3 is devoted to the construction of the two-soliton solution. In Section 4, an asymptotic analysis of the two-soliton solution is performed to reveal the interaction characteristics of solitons. Section 5 focuses on the modulational instability of the system under variable-coefficient conditions. Finally, Section 6 summarizes the main results and concludes the paper.

2. Bilinear form and one-soliton solution for the variable-coefficient CS-KdV equations

For the variable-coefficient CS-KdV equations, we first introduce the following dependent variable transformation, which is commonly used in soliton theory[8]

$$q(x,t)=\frac{G(x,t)}{F(x,t)},\quad w(x,t)=2(\ln F(x,t))_{xx}. \tag{2}$$

Here, $G(x,t)$ is a complex differentiable function and $F(x,t)$ is a real function. Under the supplementary conditions $a(t)=b(t)$ and $c(t)=d(t)$, the bilinear form of Eq. (1) is derived as

$$\begin{aligned}&\left[\mathrm{i}D_t-a(t)D_x^2\right]G(x,t)\cdot F(x,t)=0,\\&\left[2D_xD_t+d(t)D_x^4\right]F(x,t)\cdot F(x,t)=l^2(t)G(x,t)\cdot G(x,t)^*.\end{aligned} \tag{3}$$

The superscript "$*$" denotes the complex conjugate, and the Hirota bilinear differential operator D is defined as

$$\begin{aligned}&D_x^mD_t^n(a\cdot b)\\&=\left(\frac{\partial}{\partial x}-\frac{\partial}{\partial x'}\right)^m\left(\frac{\partial}{\partial t}-\frac{\partial}{\partial t'}\right)^n a(x,t)b(x',t')\Big|_{x'=x,t'=t},\end{aligned} \tag{4}$$

where m and n are integers.

The following power series expansions in the parameter ε are used to solve for the functions $F(x,t)$ and $G(x,t)$ in the bilinear form:

$$F(x,t)=1+\varepsilon^2f_2(x,t)+\varepsilon^4f_4(x,t)+\cdots, \tag{5}$$

$$G(x,t)=\varepsilon g_1(x,t)+\varepsilon^3g_3(x,t)+\cdots, \tag{6}$$

where ε is a real parameter. By substituting Eqs. (5) and (6) into Eq. (3) and setting the coefficients of different powers of ε to zero, where g_n (for $n=1,3,5,\ldots$) are complex functions of x and t, and f_m (for $m=2,4,6,\ldots$) are real functions. The resulting equations are

$$[2D_xD_t+d(t)D_x^4]1\cdot 1=0, \tag{7}$$

$$[\mathrm{i}D_t-a(t)D_x^2]g_1(x,t)\cdot 1=0, \tag{8}$$

$$\begin{aligned}&[2D_xD_t+d(t)D_x^4](f_2(x,t)\cdot 1+1\cdot f_2(x,t))\\&=l^2(t)g_1(x,t)g_1^*(x,t),\end{aligned} \tag{9}$$

$$[\mathrm{i}D_t-a(t)D_x^2](g_1(x,t)\cdot f_2(x,t)+g_3(x,t)\cdot 1)=0. \tag{10}$$

To obtain the one-soliton solution of the equation, the functions $G(x,t)$ and $F(x,t)$ are truncated as follows:[8]

$$G(x,t)=\varepsilon g_1(x,t),\quad F(x,t)=1+\varepsilon^2f_2(x,t). \tag{11}$$

It is assumed that

$$g_1(x,t)=\mathrm{e}^{\eta_1}, \tag{12}$$

where $\eta_1=k_1x+\omega_1(t)+\eta_1^0$, the parameter k_1 is a complex constant, $\omega_1(t)$ is a complex function of t, and η_1^0 is the complex phase constant of η_1. Upon substitution, we obtain the following result:

$$\omega_1(t)=-\mathrm{i}k_1^2\int a(t)\,\mathrm{d}t. \tag{13}$$

Equation (13) shows that the temporal coefficient $a(t)$ directly affects the phase evolution of the nonlinear wave. Since the phase term determines the propagation characteristics of the soliton, including its velocity and trajectory, the time-dependent coefficient introduces a dynamic modulation to the wave motion. As a result, the soliton velocity is no longer constant but may vary during propagation, which reflects the influence of an inhomogeneous medium on nonlinear wave dynamics.

$$f_2(x,t)=M\mathrm{e}^{\eta_1+\eta_1^*}, \tag{14}$$

where

$$M=\frac{l^2(t)}{-4\mathrm{i}a(t)(k_1+k_1^*)^2(k_1-k_1^*)+2d(t)(k_1+k_1^*)^4}. \tag{15}$$

By imposing the conditions

$$d(t)=2l^2(t),\quad a(t)=\mathrm{i}l^2(t)(k_1+k_1^*), \tag{16}$$

the expression for M simplifies to

$$M=\frac{1}{8k_1(k_1+k_1^*)^3}. \tag{17}$$

Setting $\varepsilon=1$ and substituting the above results, the one-soliton solution is obtained as

$$\begin{aligned}q(x,t)&=\frac{\mathrm{e}^{\eta_1}}{1+M\mathrm{e}^{\eta_1+\eta_1^*}},\\w(x,t)&=2[\ln(1+M\mathrm{e}^{\eta_1+\eta_1^*})]_{xx}.\end{aligned} \tag{18}$$

Alternatively, the one-soliton solution can be expressed in the following standard form as referenced in Refs. [23,24]:

$$\begin{cases}q(x,t)=\frac{\mathrm{e}^{\eta_1}}{1+M\mathrm{e}^{\eta_1+\eta_1^*}}=\frac{\mathrm{e}^{\mathrm{i}\eta_{1I}}}{2\mathrm{e}^{\frac{\ln M}{2}}}\operatorname{sech}\left(\eta_{1R}+\frac{\ln M}{2}\right),\\w(x,t)=2\left[\ln\left(1+M\mathrm{e}^{\eta_1+\eta_1^*}\right)\right]_{xx}\\\qquad=\frac{\left(k_1+k_1^*\right)^2}{2}\operatorname{sech}^2\left(\eta_{1R}+\frac{\ln M}{2}\right).\end{cases} \tag{19}$$

The obtained one-soliton solution exhibits a localized structure, enabling a direct analytical characterization of its key physical properties.

The propagation velocity of the soliton is determined by the phase function $\eta_1=k_1x+\omega_1(t)$. By imposing the invariant condition $\mathrm{d}\eta_1/\mathrm{d}t=0$, one obtains

$$V(t)=-\frac{\omega_1'(t)}{k_1}.$$

Using Eq. (13), it follows that

$$V(t)=\mathrm{i}k_1a(t),$$

which shows that the soliton velocity is directly modulated by the variable coefficient $a(t)$. Since k_1 is a complex parameter, the real part of $V(t)$ corresponds to the physical propagation velocity.

The soliton width is determined by the spatial decay behavior of the solution, which is governed by the real part of η_1. Thus, the width can be expressed as

$$W = 1/\mathrm{Re}(k_1),$$

this indicates that the real part of k_1 controls the localization degree of the soliton.

The amplitude (wave height) of the soliton can be obtained from the maximum value of $w(x,t)$ in Eq. (19), which yields

$$A = (k_1 + k_1^*)^2/2,$$

this shows that the amplitude depends on both the real and imaginary parts of the complex parameter k_1.

From the above results, it is clear that the variable coefficient $a(t)$ plays a crucial role in controlling the soliton velocity, while the parameter k_1 determines both the amplitude and width. Therefore, the variable-coefficient system provides an effective mechanism for manipulating the propagation, amplitude, and localization of nonlinear waves in inhomogeneous media.

Figure 1 illustrates the three-dimensional structure of the one-soliton solution obtained from Eq. (18) under the exponential coefficient $a(t) = \mathrm{e}^t$. The waveform exhibits a typical localized bell-shaped soliton structure with a single dominant peak. The amplitude reaches its maximum at the center of the wave packet and gradually decreases as the spatial distance increases. During the propagation process, the soliton maintains a stable and coherent profile without significant distortion, which reflects the intrinsic stability of nonlinear solitary waves. The exponential coefficient enhances the localization of the soliton and results in a sharper amplitude peak, indicating that the external potential plays an important role in controlling the spatial concentration of the wave energy.

Figure 2 presents the one-soliton solution in the quadratic potential field $a(t) = t^2$. Compared with Fig. 1, the waveform shows a noticeable S-shaped deformation in the spatial profile. The wavefront and waveback become asymmetric, indicating that the quadratic temporal coefficient introduces nonuniform modulation to the propagation of the soliton. Although the shape of the wave packet is slightly distorted, the localized structure of the soliton remains preserved. This result demonstrates that the quadratic potential field significantly affects the propagation characteristics and spatial distribution of the nonlinear wave.

Figure 3 depicts the evolution of the one-soliton solution under the trigonometric coefficient $a(t) = \sin t$. The wave profile exhibits a periodically modulated structure along the propagation direction. Multiple wave peaks appear in a regular pattern, forming a periodic soliton structure. This oscillatory behavior results from the periodic nature of the trigonometric potential, which introduces time-dependent modulation into the nonlinear wave system. Consequently, both the amplitude and spatial distribution of the soliton vary periodically during propagation.

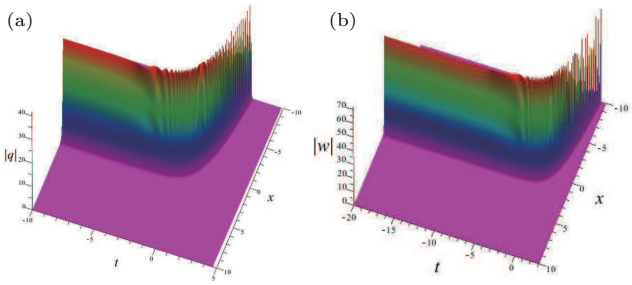


Fig. 1. Plots of the one-soliton solution via Eq. (18) with $k_1 = 6 + 0.5\mathrm{i}$, $\eta_1^0 = 0$, $a(t) = \mathrm{e}^t$.

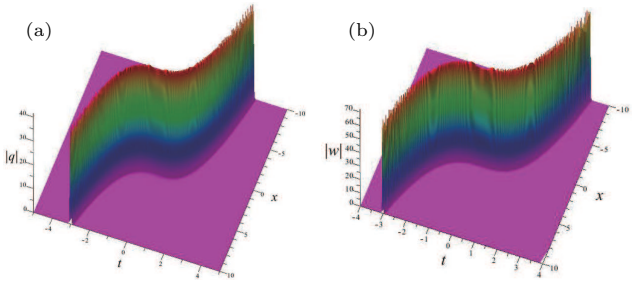


Fig. 2. Plots of the one-soliton solution via Eq. (18) with $k_1 = 6 + 0.5\mathrm{i}$, $\eta_1^0 = 0$, $a(t) = t^2$.

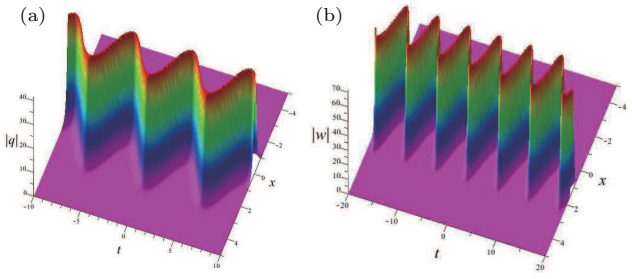


Fig. 3. Plots of the one-soliton solution via Eq. (18) with $k_1 = 6 + 0.5\mathrm{i}$, $\eta_1^0 = 0$, $a(t) = \sin t$.

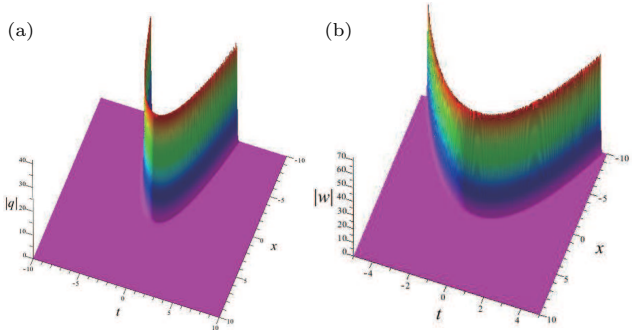


Fig. 4. Plots of the one-soliton solution via Eq. (18) with $k_1 = 6 + 0.5\mathrm{i}$, $\eta_1^0 = 0$, $a(t) = t$.

Figure 4 shows the soliton dynamics in the linear potential field $a(t)=t$. The waveform displays a tilted soliton structure in which the wave peak gradually shifts along the spatial direction over time. The wavefront and waveback exhibit clear asymmetry, and the soliton profile undergoes continuous deformation during propagation. This phenomenon indicates that the linear temporal coefficient introduces a drift effect on the soliton propagation. As a result, the propagation velocity and spatial trajectory of the soliton are continuously modified by the external linear potential.

In all cases, the parameters remain constant: $k_1 = 6+0.5\mathrm{i}$, $\eta_1^0 = 0$. The color mapping scheme consistently uses a blue-red gradient color scale, where warm colors represent high-amplitude regions and cool colors represent low-amplitude regions. The results demonstrate that different functional forms of the potential significantly influence the spatial localization, symmetry, and propagation characteristics of the soliton solutions, providing an intuitive basis for understanding the controllability of soliton behavior in nonlinear systems.

From the obtained one-soliton solution, it can be observed that the amplitude, width, and propagation velocity of the soliton are significantly influenced by the time-dependent coefficients. Physically, these coefficients can describe varying dispersion and nonlinear effects in inhomogeneous media. As a result, the soliton profile can undergo compression, stretching, or amplitude modulation during propagation. Such controllable characteristics are particularly important in nonlinear optical fibers and plasma systems, where variable environmental parameters may influence wave evolution.

3. Two-soliton solutions and their interactions for the variable-coefficient CS-KdV equations

To derive the two-soliton solutions for Eq. (1), the functions $G(x,t)$ and $F(x,t)$ are expanded as follows:

$$F(x,t) = 1+\varepsilon^2 f_2(x,t)+\varepsilon^4 f_4(x,t), \tag{20}$$

$$G(x,t) = \varepsilon g_1(x,t)+\varepsilon^3 g_3(x,t). \tag{21}$$

We assume

$$g_1(x,t) = \mathrm{e}^{\eta_1}+\mathrm{e}^{\eta_2}, \tag{22}$$

where $\eta_j = k_j x+\omega_j(t)+\eta_j^0$ for $j=1,2$, with k_j and ω_j being complex parameters, and η_j^0 representing the complex phase constants of η_j. Substituting Eq. (22) into Eq. (3), we obtain

$$\omega_j(t) = -\mathrm{i}k_j^2\int a(t)\mathrm{d}t. \tag{23}$$

Substituting Eq. (22) into Eq. (9) leads to the following expression for $f_2(x,t)$:

$$\begin{aligned} f_2(x,t) \;=\; & M_{11}\,\mathrm{e}^{\eta_1+\eta_1^*}+M_{12}\,\mathrm{e}^{\eta_1+\eta_2^*} \\ & +M_{21}\,\mathrm{e}^{\eta_2+\eta_1^*}+M_{22}\,\mathrm{e}^{\eta_2+\eta_2^*}, \end{aligned} \tag{24}$$

where the coefficients M_{ij} are defined as

$$M_{11} = \frac{l^2(t)}{-4\mathrm{i}a(t)\left(k_1+k_1^*\right)^2\left(k_1-k_1^*\right)+2d(t)\left(k_1+k_1^*\right)^4},$$

$$M_{12} = \frac{l^2(t)}{-4\mathrm{i}a(t)\left(k_1+k_2^*\right)^2\left(k_1-k_2^*\right)+2d(t)\left(k_1+k_2^*\right)^4},$$

$$M_{21} = \frac{l^2(t)}{-4\mathrm{i}a(t)\left(k_2+k_1^*\right)^2\left(k_2-k_1^*\right)+2d(t)\left(k_2+k_1^*\right)^4},$$

$$M_{22} = \frac{l^2(t)}{-4\mathrm{i}a(t)\left(k_2+k_2^*\right)^2\left(k_2-k_2^*\right)+2d(t)\left(k_2+k_2^*\right)^4}.$$

Furthermore, the variable coefficients $a(t)$ and $d(t)$ are assumed to satisfy the following relations:

$$a(t) = \mathrm{i}ml^2(t),\;\; d(t) = nl^2(t),$$

where m and n are constants. Consequently, the following expressions are derived:

$$g_3(x,t) \;=\; N_{11}\,\mathrm{e}^{\eta_1+\eta_2+\eta_1^*}+N_{12}\,\mathrm{e}^{\eta_1+\eta_2+\eta_2^*}, \tag{25}$$

$$\begin{aligned} f_4(x,t) \;=\; & B_1\,\mathrm{e}^{2\eta_1+\eta_1^*+\eta_2^*}+B_2\,\mathrm{e}^{2\eta_2+\eta_1^*+\eta_2^*} \\ & +B_3\,\mathrm{e}^{2\eta_1^*+\eta_1+\eta_2}+B_4\,\mathrm{e}^{2\eta_2^*+\eta_1+\eta_2} \\ & +B_5\,\mathrm{e}^{\eta_1+\eta_2+\eta_1^*+\eta_2^*}, \end{aligned} \tag{26}$$

with the coefficients defined as

$$N_{11} = \frac{M_{21}(k_1-k_2)(k_1^*+k_2)+M_{11}(k_2-k_1)(k_1+k_1^*)}{(k_1+k_1^*)(k_1^*+k_2)},$$

$$N_{12} = \frac{M_{22}(k_1-k_2)(k_2^*+k_2)+M_{12}(k_2-k_1)(k_1+k_2^*)}{(k_2+k_1^*)(k_2^*+k_1)},$$

$$B_1 = \frac{N_{11}^*+4mM_{11}M_{12}(k_1^*-k_2^*)(k_1^{*2}-k_2^{*2})-2nM_{11}M_{12}(k_1^*-k_2^*)}{4m(2k_1^2-k_1^{*2}-k_2^{*2})(2k_1+k_1^*+k_2^*)+2n(2k_1+k_1^*+k_2^*)^4},$$

$$B_2 = \frac{N_{12}^*+4mM_{21}M_{22}(k_1^*-k_2^*)(k_1^{*2}-k_2^{*2})-2nM_{21}M_{22}(k_1^*-k_2^*)}{4m(2k_2^2-k_1^{*2}-k_2^{*2})(2k_2+k_1^*+k_2^*)+2n(2k_2+k_1^*+k_2^*)^4},$$

$$B_3 = \frac{N_{11}+4mM_{11}M_{21}(k_1-k_2)(k_1^2-k_2^2)-2nM_{11}M_{21}(k_1-k_2)}{4m(2k_1^{2*}-k_1^2-k_2^2)(2k_1^*+k_1+k_2)+2n(2k_1^*+k_1+k_2)^4},$$

$$B_4 = \frac{N_{12}+4mM_{12}M_{22}(k_1-k_2)(k_1^2-k_2^2)-2nM_{12}M_{22}(k_1-k_2)}{4m(2k_2^{2*}-k_1^2-k_2^2)(2k_2^*+k_1+k_2)+2n(2k_2^*+k_1+k_2)^4},$$

$$\begin{aligned} S_1 = M_{11}M_{22}\Big[& 4m(k_1+k_1^*-k_2-k_2^*)(k_1^2+k_1^{*^2}-k_2^2-k_2^{*^2}) \\ & +2n(k_1+k_1^*-k_2-k_2^*)^4\Big], \end{aligned}$$

$$\begin{aligned} S_2 = {} & 4m(k_1+k_1^*+k_2+k_2^*)(k_1^2+k_2^2-k_1^{*^2}-k_2^{*^2}) \\ & +2n(k_1+k_1^*+k_2+k_2^*)^4, \end{aligned}$$

$$\begin{aligned} S_3 = M_{21}M_{12}\Big[& 4m(k_1+k_2^*-k_2-k_1^*)(k_1^2+k_2^{*^2}-k_2^2-k_1^{*^2}) \\ & +2n(k_1+k_2^*-k_2-k_1^*)^4\Big], \end{aligned}$$

$$B_5 = -\frac{S_1}{S_2}-\frac{S_3}{S_2}.$$

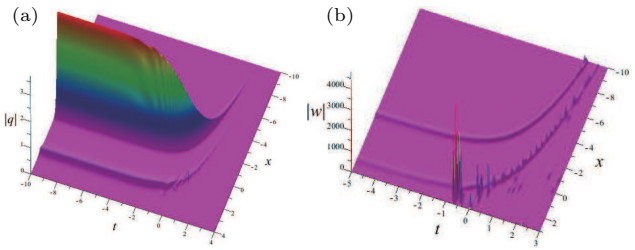


Fig. 5. Two-soliton solutions obtained from Eq. (27) with $k_1 = 6+0.5\mathrm{i}$, $k_2 = -5+0.4\mathrm{i}$, $\eta_1^0 = 0$, $\eta_2^0 = 0$, $m = 1$, $n = 1$, $a(t) = \mathrm{e}^t$.

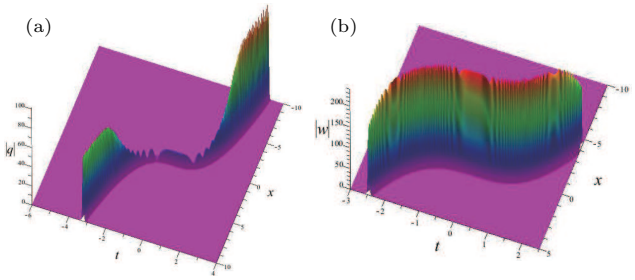


Fig. 6. Two-soliton solutions obtained from Eq. (27) with $k_1 = 6+0.5\mathrm{i}$, $k_2 = 6-0.5\mathrm{i}$, $\eta_1^0 = 0$, $\eta_2^0 = 0$, $m = 1$, $n = 1$, $a(t) = t^2$.

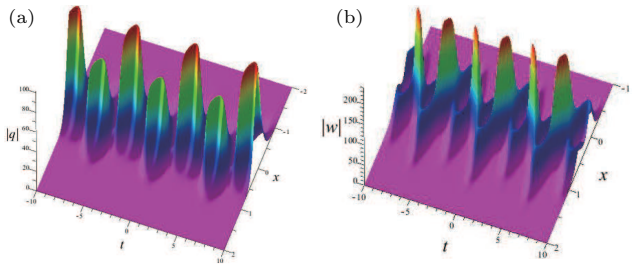


Fig. 7. Two-soliton solutions obtained from Eq. (27) with $k_1 = 6+0.5\mathrm{i}$, $k_2 = 5-0.4\mathrm{i}$, $\eta_1^0 = 0$, $\eta_2^0 = 0$, $m = 1$, $n = 1$, $a(t) = \sin t$.

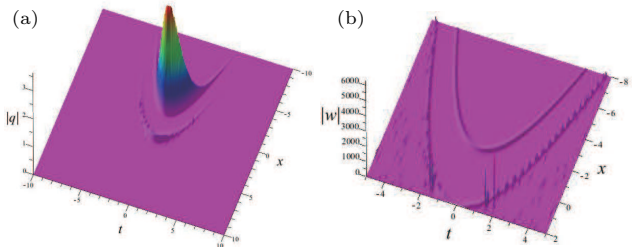


Fig. 8. Two-soliton solutions obtained from Eq. (27) with $k_1 = 6+0.5\mathrm{i}$, $k_2 = -5+0.4\mathrm{i}$, $\eta_1^0 = 0$, $\eta_2^0 = 0$, $m = 1$, $n = 1$, $a(t) = t$.

Setting $\varepsilon = 1$ and substituting Eqs. (20)–(26) into Eq. (2), the two-soliton solutions of Eq. (1) are obtained as

$$
\begin{aligned}
q(x,t) &= \frac{g_1(x,t)+g_3(x,t)}{1+f_2(x,t)+f_4(x,t)},\\
w(x,t) &= 2\left[\ln\left(1+f_2(x,t)+f_4(x,t)\right)\right]_{xx},
\end{aligned}
\tag{27}
$$

with

$$
\begin{aligned}
g_1(x,t) &= \mathrm{e}^{\eta_1}+\mathrm{e}^{\eta_2},\\
g_3(x,t) &= N_{11}\,\mathrm{e}^{\eta_1+\eta_2+\eta_1^*}+N_{12}\,\mathrm{e}^{\eta_1+\eta_2+\eta_2^*},\\
f_2(x,t) &= M_{11}\,\mathrm{e}^{\eta_1+\eta_1^*}+M_{12}\,\mathrm{e}^{\eta_1+\eta_2^*}\\
&\quad +M_{21}\,\mathrm{e}^{\eta_2+\eta_1^*}+M_{22}\,\mathrm{e}^{\eta_2+\eta_2^*},\\
f_4(x,t) &= B_1\,\mathrm{e}^{2\eta_1+\eta_1^*+\eta_2^*}+B_2\,\mathrm{e}^{2\eta_2+\eta_1^*+\eta_2^*}\\
&\quad +B_3\,\mathrm{e}^{2\eta_1^*+\eta_1+\eta_2}+B_4\,\mathrm{e}^{2\eta_2^*+\eta_1+\eta_2}\\
&\quad +B_5\,\mathrm{e}^{\eta_1+\eta_2+\eta_1^*+\eta_2^*}.
\end{aligned}
$$

The two-soliton solution in Eq. (27) describes the interaction dynamics of two coexisting solitons in the coupled system. The interference term $g_3(x,t)$ and potential terms $f_2(x,t), f_4(x,t)$ encode the nonlinear collision process, confirming the elastic nature of soliton interactions — solitons retain their original amplitudes and velocities after collision, a key feature of integrable systems. Time-dependent coefficients $a(t)$ and $d(t)$ tune the collision region and interference pattern, enabling diverse soliton interaction behaviors. The $w(x,t)$ potential dynamically mediates energy transfer during collision and restores to a dual-well structure afterward, highlighting the long-wave component's role in stabilizing multi-soliton propagation. To investigate the dynamical properties, numerical simulations are performed with different coefficient selections, yielding the results depicted in Figs. 5–8.

Figure 5 illustrates the three-dimensional structure of the two-soliton solution under the exponential coefficient $a(t) = \mathrm{e}^t$. The corresponding wave profiles exhibit two distinct localized structures characterized by relatively flat plateau regions and sharp gradient transitions along the spatial direction. Such profiles resemble kink-type or step-like structures rather than standard bell-shaped solitons. This behavior can be attributed to the exponential growth of $a(t)$, which enhances the effective nonlinear interaction and leads to a rapid steepening of the wavefronts. As a result, the wave energy becomes increasingly concentrated near the transition regions, producing sharper spatial localization. Moreover, the two localized structures remain spatially separated during evolution, indicating that the exponential coefficient mainly affects the steepness and localization rather than inducing strong waveform deformation.

Figure 6 presents the two-soliton solution under the quadratic coefficient $a(t) = t^2$. In this case, the wave profiles exhibit pronounced asymmetry and significant deformation. One of the structures develops a narrow and steep peak, while the other becomes broader and smoother, leading to an overall S-shaped spatial configuration. This phenomenon reflects the nonuniform modulation introduced by the quadratic coefficient, where the effective dispersion and nonlinearity vary with time. Consequently, the amplitudes and widths of the wave packets are no longer constant but evolve dynamically, resulting in stretching, compression, and distortion of the waveforms. Compared with the exponential case, the quadratic coefficient produces stronger deformation effects and a more extended spatial distribution, indicating a higher degree of controllability over the wave structure.

Figure 7 shows the two-soliton solution under the trigonometric coefficient $a(t) = \sin t$. The corresponding wave profiles display a pronounced periodic pattern consisting of multiple regularly spaced peaks along the spatial direction. Instead of isolated localized structures, the solution forms a wave train with alternating high- and low-amplitude regions. This behavior is a direct consequence of the oscillatory nature of $a(t)$, which periodically modulates both the effective nonlinearity and dispersion. As a result, the amplitudes of the peaks vary synchronously with time, and the overall structure exhibits periodic repetition. This indicates that the trigonometric coefficient can transform localized soliton-like structures into spatially extended, periodically modulated wave patterns.

Figure 8 presents the three-dimensional structure of the two-soliton solution under the linear coefficient $a(t) = t$, with parameters $k_1 = 6 + 0.5\mathrm{i}$, $k_2 = -5 + 0.4\mathrm{i}$. The two-soliton wave packets propagate with linearly varying velocities, leading to an asymmetric collision structure where the interaction occurs at a non-central spatial position. The amplitudes of the solitons change linearly with time, with one soliton showing a gradual increase in amplitude while the other decreases, reflecting the linear potential's effect on wave energy evolution. After interaction, the solitons maintain their localized shapes but exhibit modified velocity and amplitude trends, indicating that the linear potential continuously modulates the soliton dynamics throughout propagation and collision. This result reveals the possibility of precisely tuning soliton collision parameters via linear time-dependent coefficients.

All these simulations are based on the two-soliton solutions of Eq. (27) with fixed parameters $\eta_1^0 = 0$, $\eta_2^0 = 0$ and $m = n = 1$, and a consistent blue-red color map is adopted for visualization. In this color map, warm colors represent high-amplitude regions while cool colors represent low-amplitude regions. The results demonstrate that different functional forms of the potential significantly influence the collision dynamics of the two solitons, including the interaction strength, energy exchange mechanisms, and waveform evolution characteristics.[25] This work provides clear visual insight for understanding multi-soliton interactions in nonlinear systems.

For the two-soliton solution, the interaction between two localized wave packets demonstrates the typical elastic interaction property of solitons. Although the solitons may experience phase shifts during interaction, their shapes and velocities remain unchanged after the collision. This property indicates the stability of nonlinear wave structures governed by the coupled Schrödinger-KdV system. In physical systems such as optical waveguides or plasma environments, this stability is essential for maintaining signal integrity during wave propagation.

4. Asymptotic analysis

Solitons are localized waves that propagate without distortion. The investigation of soliton collisions is fundamentally important for understanding nonlinear dynamical systems.[23] The coupled variable-coefficient Schrödinger-KdV equations play a key role in modeling wave interactions within inhomogeneous media. This analysis begins by examining the asymptotic behavior of the two-soliton solution, which is organized into the following cases.

(1) Before collision ($t \to -\infty$)

(a) ($\eta_{1\mathrm{R}} \approx 0, \eta_{2\mathrm{R}} \to -\infty$)

$$\begin{aligned} q \to q_1^- &= \frac{\mathrm{e}^{\eta_1}}{1 + M_{11}\,\mathrm{e}^{\eta_1+\eta_1^*}} \\ &= \frac{\mathrm{e}^{\mathrm{i}\eta_{1\mathrm{I}}}}{2\,\mathrm{e}^{\frac{\ln M_{11}}{2}}}\operatorname{sech}\left(\eta_{1\mathrm{R}} + \frac{\ln M_{11}}{2}\right), \\ w \to w_1^- &= 2\left[\ln\left(1 + M_{11}\,\mathrm{e}^{\eta_1+\eta_1^*}\right)\right]_{xx} \\ &= \frac{(k_1 + k_1^*)^2}{2}\operatorname{sech}^2\left(\eta_{1\mathrm{R}} + \frac{\ln M_{11}}{2}\right). \end{aligned}$$

(b) ($\eta_{2\mathrm{R}} \approx 0, \eta_{1\mathrm{R}} \to -\infty$)

$$\begin{aligned} q \to q_2^- &= \frac{\mathrm{e}^{\eta_2}}{1 + M_{22}\,\mathrm{e}^{\eta_2+\eta_2^*}} \\ &= \frac{\mathrm{e}^{\mathrm{i}\eta_{2\mathrm{I}}}}{2\,\mathrm{e}^{\frac{\ln M_{22}}{2}}}\operatorname{sech}\left(\eta_{2\mathrm{R}} + \frac{\ln M_{22}}{2}\right), \\ w \to w_2^- &= 2\left[\ln\left(1 + M_{22}\,\mathrm{e}^{\eta_2+\eta_2^*}\right)\right]_{xx} \\ &= \frac{(k_2 + k_2^*)^2}{2}\operatorname{sech}^2\left(\eta_{2\mathrm{R}} + \frac{\ln M_{22}}{2}\right). \end{aligned}$$

Figures 9(a) and 9(b) display the images for $k_1 = 6 + 0.5\mathrm{i}$, $k_2 = -5 + 0.4\mathrm{i}$, $\eta_1^0 = \eta_2^0 = 0$, $m = n = 1$, $a(t) = \mathrm{e}^t$. In Fig. 9(a), when time is far from zero (e.g., $t < -10$), the parameter $|q|$ is maintained at an extremely low and nearly constant level (approximately 0.0002). Correspondingly, in Fig. 9(b), within the same temporal region, the amplitude $|w|$ remains at a relatively high and stable value (approximately 0.0008). This state corresponds to the two solitons being widely separated in space with no significant interaction. The coupling effect between them is negligible, while the amplitude of their respective localized wave packets remains pronounced.

(2) After collision ($t \to \infty$)

(a) ($\eta_{1\mathrm{R}} \approx 0, \eta_{2\mathrm{R}} \to \infty$)

$$\begin{aligned} q \to q_1^+ &= \frac{N_{12}\,\mathrm{e}^{\eta_1}}{B_2\,\mathrm{e}^{\eta_2+\eta_1^*} + B_4\,\mathrm{e}^{\eta_1+\eta_2^*}} \\ &= \frac{\mathrm{e}^{\mathrm{i}\eta_{1\mathrm{I}}}}{2}\,\mathrm{e}^{\ln N_{12} - (\eta_{2\mathrm{R}} + \frac{\ln B_2}{2} + \frac{\ln B_4}{2})} \\ &\quad \times \operatorname{sech}\left(\mathrm{i}\eta_{1\mathrm{I}} - \mathrm{i}\eta_{2\mathrm{I}} + \frac{\ln B_2}{2} - \frac{\ln B_4}{2}\right), \end{aligned}$$

$$w \to w_1^+ = 2\left[\ln\left(B_2\,\mathrm{e}^{\eta_2+\eta_1^*}+B_4\,\mathrm{e}^{\eta_1+\eta_2^*}\right)\right]_{xx}$$

$$= \frac{2\left(B_2\,(k_2+k_1^*)^2\,\mathrm{e}^{\eta_2+\eta_1^*}+B_4\,(k_1+k_2^*)^2\,\mathrm{e}^{\eta_1+\eta_2^*}\right)}{B_2\,\mathrm{e}^{\eta_2+\eta_1^*}+B_4\,\mathrm{e}^{\eta_1+\eta_2^*}} - \frac{2\left(B_2\,(k_2+k_1^*)\,\mathrm{e}^{\eta_2+\eta_1^*}+B_4\,(k_1+k_2^*)\,\mathrm{e}^{\eta_1+\eta_2^*}\right)^2}{\left(B_2\,\mathrm{e}^{\eta_2+\eta_1^*}+B_4\,\mathrm{e}^{\eta_1+\eta_2^*}\right)^2}$$

$$= 2\ln\left(B_2\,\mathrm{e}^{\eta_2+\eta_1}+B_4\,\mathrm{e}^{\eta_1+\eta_2^*}\right) \times\operatorname{sech}\left(\mathrm{i}\eta_1\eta_2+\frac{\ln B_2}{2}-\frac{\ln B_4}{2}\right).$$

(b) $(\eta_{1\mathrm{R}}\to\infty, \eta_{2\mathrm{R}}\approx 0)$

$$q \to q_2^+ = \frac{N_{11}\,\mathrm{e}^{\eta_2}}{B_1\,\mathrm{e}^{\eta_1+\eta_2^*}+B_3\,\mathrm{e}^{\eta_2+\eta_1^*}}$$

$$= \frac{\mathrm{e}^{\mathrm{i}\eta_{2\mathrm{I}}}}{2}\,\mathrm{e}^{\,\mathrm{i}nN_{11}-\left(\eta_{1\mathrm{I}}+\frac{\ln B_1}{2}+\frac{\ln B_3}{2}\right)} \times\operatorname{sech}\left(\mathrm{i}\eta_{2\mathrm{I}}-\mathrm{i}\eta_{1\mathrm{I}}+\frac{\ln B_1}{2}-\frac{\ln B_3}{2}\right),$$

$$w \to w_2^+ = 2\left[\ln\left(B_1\,\mathrm{e}^{\eta_1+\eta_2^*}+B_3\,\mathrm{e}^{\eta_2+\eta_1^*}\right)\right]_{xx}$$

$$= \frac{2\left(B_1\,(k_1+k_2^*)^2\,\mathrm{e}^{\eta_1+\eta_2^*}+B_3\,(k_2+k_1^*)^2\,\mathrm{e}^{\eta_2+\eta_1^*}\right)}{B_1\,\mathrm{e}^{\eta_1+\eta_2^*}+B_3\,\mathrm{e}^{\eta_2+\eta_1^*}} - \frac{2\left(B_1\,(k_1+k_2^*)\,\mathrm{e}^{\eta_1+\eta_2^*}+B_3\,(k_2+k_1^*)\,\mathrm{e}^{\eta_2+\eta_1^*}\right)^2}{\left(B_1\,\mathrm{e}^{\eta_1+\eta_2^*}+B_3\,\mathrm{e}^{\eta_2+\eta_1^*}\right)^2}$$

$$= 2\ln\left(B_1\,\mathrm{e}^{\eta_1+\eta_2}+B_3\,\mathrm{e}^{\eta_2+\eta_1^*}\right) \times\operatorname{sech}\left(\mathrm{i}\eta_1\eta_2+\frac{\ln B_1}{2}-\frac{\ln B_3}{2}\right),$$

where $\eta_{j\mathrm{R}}$ and $\eta_{j\mathrm{I}}$ denote the real part and imaginary part of η_j, respectively, and $j=1,2$.

Figure 10(a) displays the images for $k_1=6+0.5\mathrm{i}$, $k_2=6-0.5\mathrm{i}$, $\eta_1^0=\eta_2^0=0$, $m=n=1$, $a(t)=t^2$. In the late stage of system evolution ($t\to+\infty$), the value of $|q|$ decays monotonically, tending to zero as time increases. Figure 10(b) displays the images for $k_1=6+0.5\mathrm{i}$, $k_2=5-0.4\mathrm{i}$, $\eta_1^0=\eta_2^0=0$, $m=n=1$, $a(t)=\sin t$. In the late stage of system evolution ($t\to+\infty$), the value of $|q|$ exhibits a distinct periodic distribution pattern. The emergence of this periodicity indicates that the system has reached a dynamic equilibrium state after the completion of soliton interactions, rather than a static steady state.

The time-dependent coefficients modulate this interaction, highlighting the controllability offered by variable-coefficient models,[6,12] a significant advantage over constant-coefficient counterparts with direct implications for signal shaping in optics.[26] The asymptotic analysis further confirms that although the interaction remains elastic in structure, the propagation characteristics before and after collision are modulated by the time-dependent coefficients, which distinguishes the present model from the classical constant-coefficient case. As shown in Figs. 9 and 10, as $t\to\pm\infty$, the two-soliton solution gradually decomposes into two independent solitary waves. Each soliton preserves its amplitude and velocity after the interaction, which confirms the elastic nature of the soliton collision in the variable-coefficient system.

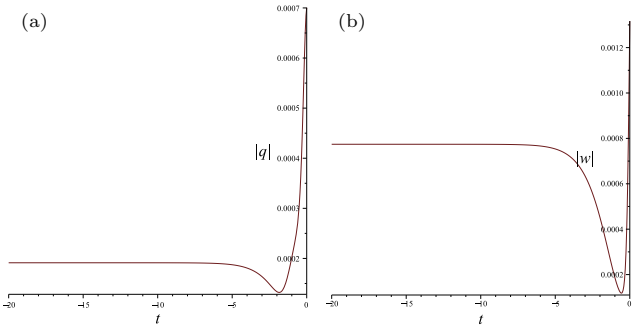


Fig. 9. Asymptotic behavior of the solution presented in Eq. (27).

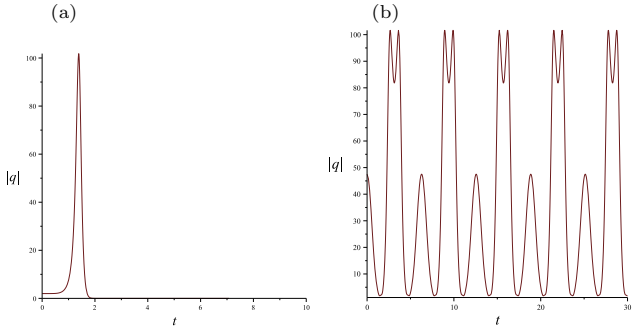


Fig. 10. Asymptotic behavior of the solution presented in Eq. (27).

5. Modulation instability on the autonomous soliton solutions

Modulational instability (MI) is a core physical phenomenon in nonlinear dispersive systems, induced by the combined effects of nonlinearity and dispersion. It is characterized by the spontaneous amplification of initial weak perturbations, ultimately leading to abrupt system state changes such as pulse splitting and spectral broadening.[27] Widely existing in fields like optical fiber communication, Bose–Einstein condensates (BECs), and metamaterials, MI can induce periodic modulation of matter-wave density in BEC systems — especially in spin–orbit coupled binary BECs confined to deep optical lattices, where spin–orbit coupling and inter/intra-species nonlinearity play distinct critical roles in shaping instability landscapes.[28–31] This makes MI a key entry point to reveal the laws of quantum many-body systems, with implications for quantum simulation and quantum information processing.[28,31,32] In metamaterials, MI induced by cross-phase modulation exhibits distinct characteristics from that in traditional media, attributed to their artificially designed microstructures and unique electromagnetic properties, which enhance nonlinear light–matter interactions and provide new ideas for advanced optical device design.[30,31] As the core

mechanism for technologies such as supercontinuum generation, which relies on the complex interplay between MI, self-phase modulation, and dispersion in optical fibers, MI remains a long-standing research hotspot in nonlinear science.[4,25] Recent advances have further extended MI research to complex systems, including discrete (optical lattices) where periodic potential fields significantly alter instability thresholds and growth rates, opening new avenues for nonlinear dynamics.[29]

We set $c(t)=d(t)=2l^2(t)=2$, $a(t)=b(t)=\mathrm{i}(k_1+k_1^*)$, and $\eta_1^0=0$. Subsequently, small perturbations are introduced into Eq. (19), yielding the modified equations

$$q_{11}=q(x,t)\left(1+f_1\,\mathrm{e}^{\mathrm{i}(\kappa X-\Omega_1 T)}+f_2^*\,\mathrm{e}^{-\mathrm{i}(\kappa X-\Omega_2 T)}\right), \quad (28)$$

$$w_{11}=w(x,t)\left(1+f_3\,\mathrm{e}^{\mathrm{i}(\kappa X-\Omega_1 T)}+f_4\,\mathrm{e}^{-\mathrm{i}(\kappa X-\Omega_2 T)}\right). \quad (29)$$

Here, Ω represents the complex propagation parameter, which comprehensively characterizes both the phase variation behavior and attenuation characteristics of the wave field, and f_i $(i=1,2,3,4)$ represent the small-amplitude coefficient parameters, specifically serving to quantify the time-varying rate of perturbation components within the system. Substituting the expressions given in Eqs. (28) and (29) into the governing Eq. (1), we can obtain the dispersion relationships between dm and Ω:

$$\begin{aligned}
&\mathrm{dm}=\frac{\mathcal{A}\cdot\mathcal{B}\cdot\mathcal{C}\cdot\mathcal{D}\cdot\mathcal{E}\cdot\mathcal{F}}{\mathcal{G}},\\
&\mathcal{AB}=-\left(8k_1^2-4k_1+1\right)^2k_1^4\left(524288\mathrm{i}k_1^{14}-3145728\mathrm{i}k_1^{13}\kappa^2\right),\\
&\mathcal{C}=64\mathrm{i}k_1^7+256\mathrm{i}k_1^6\kappa+128k_1^7+64\mathrm{i}k_1^6-128k_1^5\kappa^2\\
&\qquad+64k_1^4\Omega_1-k_1^3\mathrm{i}-4\mathrm{i}k_1^2\kappa+2k_1^3-k_1^2\mathrm{i}-2k_1\kappa^2+\Omega_1,\\
&\mathcal{D}=64\mathrm{i}k_1^7-256\mathrm{i}k_1^6\kappa+128k_1^7+64\mathrm{i}k_1^6-128k_1^5\kappa^2\\
&\qquad-64k_1^4\Omega_2-k_1^3\mathrm{i}+4\mathrm{i}k_1^2\kappa+2k_1^3-k_1^2\mathrm{i}-2k_1\kappa^2-\Omega_2,\\
&\mathcal{E}=\left(8k_1^2+4k_1+1\right)^2\mathrm{e}^{3k_1\left(k_1^2t+k_1t+x\right)},\\
&\mathcal{F}_1=524288\mathrm{i}k_1^{14}+262144k_1^{12}\Omega_1+524288k_1^{12}\kappa^3,\\
&\mathcal{F}_2=450560\mathrm{i}k_1^{11}-8192\mathrm{i}k_1^{10}-229376k_1^{10}\kappa+49152\mathrm{i}k_1^9\kappa^2,\\
&\mathcal{F}_3=-3145728\mathrm{i}k_1^{13}\kappa^2-6291456k_1^{14}\kappa\\
&\qquad-12288k_1^8\Omega_1-24576k_1^8\kappa^3,\\
&\mathcal{F}_4=18\mathrm{i}k_1^3+2\mathrm{i}k_1^2+128\mathrm{i}k_1^6-3584k_1^6\kappa+24k_1^2\kappa,\\
&\mathcal{F}_5=-384k_1^4\kappa^3-192k_1^4\Omega_1-7040\mathrm{i}k_1^7\\
&\qquad-768\mathrm{i}k_1^5\kappa^2-12\mathrm{i}k_1\kappa^2,\\
&\mathcal{F}_6=-2\kappa^3-\Omega_1,\\
&\mathcal{F}=\mathcal{F}_1+\mathcal{F}_2+\mathcal{F}_3+\mathcal{F}_4+\mathcal{F}_5+\mathcal{F}_6,\\
&\mathcal{G}=4398046511104\left(64k_1^4+\mathrm{e}^{2k_1\left(k_1^2t+k_1t+x\right)}\right)^4.
\end{aligned} \quad (30)$$

$$\Omega=\frac{\alpha+\beta+\gamma}{\delta},$$

$$\begin{aligned}
&\alpha=512\mathrm{i}k_1^5\kappa+128\mathrm{i}k_1^4\kappa^2+320k_1^6+128\mathrm{i}k_1^5,\\
&\beta=256k_1^5\kappa-256k_1^4\kappa^2+64k_1^5-4\mathrm{i}k_1^2-8\mathrm{i}k_1\kappa+2\mathrm{i}\kappa^2,\\
&\gamma=3k_1^2-2\mathrm{i}k_1-4k_1\kappa-4\kappa^2-k_1,\\
&\delta=-2+\mathrm{i}-128k_1^4+64\mathrm{i}k_1^4,
\end{aligned} \quad (31)$$

and

$$\begin{aligned}
&\Omega=-2\cdot\frac{s+t+u+v}{\Delta},\\
&s=262144\mathrm{i}k_1^{14}-3145728k_1^{14}\kappa-1572864\mathrm{i}k_1^{13}\kappa^2\\
&\qquad+262144k_1^{12}\kappa^3,\\
&t=225280\mathrm{i}k_1^{11}-4096\mathrm{i}k_1^{10}-114688k_1^{10}\kappa\\
&\qquad+24576\mathrm{i}k_1^9\kappa^2-12288k_1^8\kappa^3,\\
&u=-3520\mathrm{i}k_1^7+64\mathrm{i}k_1^6-1792k_1^6\kappa+9\mathrm{i}k_1^3+\mathrm{i}k_1^2+12k_1^2\kappa,\\
&v=-384\mathrm{i}k_1^5\kappa^2-192k_1^4\kappa^3-6\mathrm{i}k_1\kappa^2-\kappa^3,\\
&\Delta=262144k_1^{12}-12288k_1^8-192k_1^4-1.
\end{aligned} \quad (32)$$

The gain spectrum $G(\kappa)=|\mathrm{Im}(\Omega)|$ represents the growth rate of MI. When Ω possesses a nonzero imaginary part, perturbations grow exponentially, indicating the occurrence of MI. In contrast, when Ω is purely real, the perturbations remain bounded and the system is modulationally stable.

Figure 11(a) shows a three-dimensional surface plot of the modulational instability (MI) gain $G(\kappa)$ as a function of k_1 and κ. The surface exhibits a smooth distribution with distinct peaks and valleys, reflecting the variation of the instability growth rate across the parameter space. Higher regions of the surface correspond to larger values of $\mathrm{Im}(\Omega)$, indicating stronger exponential growth of perturbations, while the flat regions where the gain approaches zero correspond to stable regimes. Figure 11(b) presents a two-dimensional density plot of the MI gain. The color distribution distinguishes between stable and unstable regions: areas with zero or near-zero gain correspond to stability, whereas regions with positive gain indicate modulational instability. The stable region forms a central domain in the parameter space, while instability mainly appears near the boundaries.

Figure 12(a) shows the three-dimensional distribution of the MI gain $G(\kappa)$ as a function of k_1 and κ. Compared with Fig. 11(a), the surface exhibits more pronounced variations, with sharper peaks and steeper gradients, indicating an enhanced sensitivity of the instability growth rate to parameter changes. The regions with higher peaks correspond to stronger exponential growth of perturbations, while the flatter regions still represent stable regimes where the gain approaches zero. Figure 12(b) presents the corresponding two-dimensional density plot of the MI gain. The distribution of stable and unstable regions is clearly distinguished by the gain values: regions with near-zero gain correspond to stability, whereas regions

with positive gain indicate modulational instability. Compared with Fig. 11(b), the unstable regions become more prominent and extend further into the parameter space, suggesting that the system is more susceptible to instability under this set of conditions. This change indicates that the parameter variation enhances the growth of perturbations and reduces the stability domain.

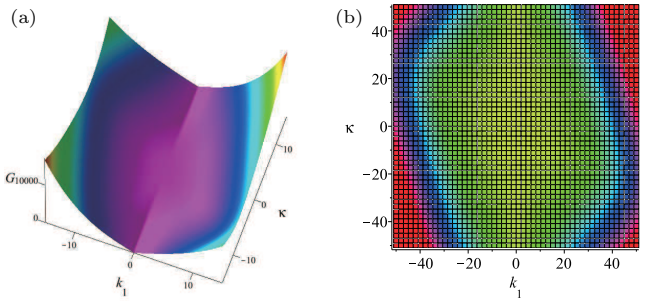


Fig. 11. Profiles of the MI gain $G(\kappa)$ with respect to k_1 and κ. (a) Three-dimensional surface plot of the MI gain. (b) Two-dimensional density plot showing the distribution of stable and unstable regions in the range $[-50,50]\times[-50,50]$.

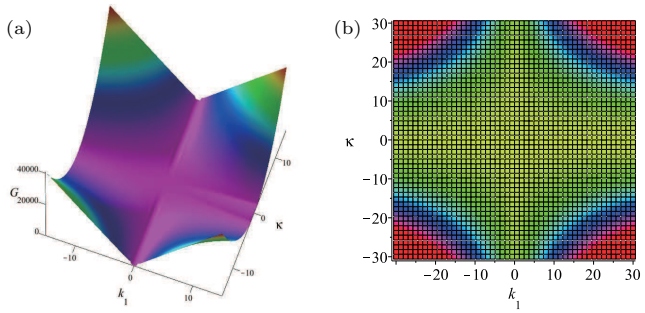


Fig. 12. Profiles of the MI gain $G(\kappa)$ with respect to k_1 and κ. (a) Three-dimensional surface plot of the MI gain. (b) Two-dimensional density plot showing the distribution of stable and unstable regions in the range $[-30,30]\times[-30,30]$.

Overall, the comparison between Figs. 11 and 12 demonstrates that the distribution of modulational instability is highly sensitive to system parameters, and the stability region can be effectively controlled by adjusting these parameters.

The dependence of the MI growth rate on the time-dependent coefficients $a(t)$, $d(t)$ and $l(t)$ indicates that MI can be either suppressed or enhanced via external parameter design. As shown in Figs. 11 and 12, the gain spectrum $G(\kappa) = |\mathrm{Im}(\Omega)|$ clearly distinguishes the stable (green/yellow) and unstable (red) regions of wave vector κ and wave number k_1, where the time-varying coefficients alter the gain peak value and unstable parameter range of the MI spectrum. Such controllability is of great significance for maintaining signal stability in advanced optical communication systems,[4,26] as it allows for the suppression of perturbation-induced pulse splitting and spectral broadening, the typical MI-induced phenomena.

MI analysis demonstrates that small perturbations imposed on the continuous-wave background may grow exponentially under specific parameter conditions of k_1 and κ.[27] The growth rate is strongly governed by time-dependent coefficients $a(t)$, $d(t)$, and $l(t)$, which suggests that the stability of nonlinear waves can be effectively controlled by tuning the temporal profiles of these system parameters. This property is particularly relevant to nonlinear optical fiber systems[25] and inhomogeneous plasma wave propagation,[22] where the regulation of MI is critical for optimizing wave transmission performance.

6. Conclusion

Using the Hirota bilinear method, this paper derives one- and two-soliton solutions for a variable-coefficient coupled Schrödinger-KdV system. The results demonstrate that time-dependent coefficients provide effective control over soliton dynamics, including amplitude, width, velocity, and interaction properties. Asymptotic analysis confirms elastic collisions in the two-soliton case under integrability conditions, while the modulational instability (MI) analysis reveals how perturbations evolve under variable-coefficient effects, highlighting stability thresholds and their practical implications for soliton-based systems. This MI analysis complements the exact soliton solutions by addressing robustness issues in realistic physical settings, such as optical communication systems and Bose–Einstein condensates. Overall, these results contribute to the theory of variable-coefficient integrable systems and indicate potential applications in inhomogeneous fiber optics and non-autonomous soliton control.

Based on the analytical framework established here, several directions merit further investigation. First, the present Hirota bilinear approach can be extended to construct higher-order N-soliton solutions ($N \geq 3$) and to explore more complex multi-soliton interaction behaviors under variable-coefficient conditions. Second, motivated by the controllability effects induced by time-dependent coefficients, inverse design of coefficient functions may be considered to realize targeted soliton evolution, such as compression and trajectory control, in accordance with nonlinear wave control theory. In addition, the methodology developed in this paper can be generalized to other variable-coefficient integrable systems, such as the VC-KP equation, allowing comparative studies of controllability mechanisms across different models. Finally, further investigations on soliton stability under perturbations or weak violations of integrability conditions are of interest for assessing practical applicability in real-world transmission systems. From a broader perspective, the present results demonstrate that variable-coefficient effects provide an additional degree of freedom for manipulating nonlinear wave dynamics. By properly designing the temporal variation of system parameters, it becomes possible to control soliton trajectories, amplitudes, and interaction behaviors. Such controllability is of

practical importance in nonlinear optics, plasma physics, and Bose–Einstein condensate systems, where external fields or inhomogeneous media often introduce time-dependent parameters. Therefore, the analytical framework developed in this work may serve as a useful tool for exploring controllable soliton dynamics in non-autonomous nonlinear systems.

Acknowledgment

Project supported by the Fundamental Research Funds for the Liaoning Universities (Grant Nos. LJ212410166016 and LJ212410166022).

References

[1] Zakharov V E and Shabat A B 1972 *Sov. Phys. JETP* **34** 62
[2] Hasegawa A and Tappert F 1973 *Appl. Phys. Lett.* **23** 142
[3] Hirota R 1973 *J. Math. Phys.* **14** 805
[4] Agrawal G P 2000 *Nonlinear Fiber Optics* (Academic Press)
[5] Özdemir C and Güngör F 2012 *Rev. Math. Phys.* **24** 1250015
[6] Serkin V N, Hasegawa A and Belyaeva T L 2007 *Phys. Rev. Lett.* **98** 074102
[7] Biswas A, Milović D and Edwards M 2010 *Mathematical Theory of Dispersion-Managed Optical Solitons* (Springer)
[8] Hirota R 1971 *Phys. Rev. Lett.* **27** 1192
[9] Yu J and Yu F 2026 *Appl. Math. Lett.* **174** 109827
[10] Zhou M and Yu F 2026 *Appl. Math. Lett.* **178** 109937
[11] Gardner C S, Greene J M, Kruskal M D and Miura R M 1967 *Phys. Rev. Lett.* **19** 1095
[12] Wael S, Maowad S M and El-Kalaawy O H 2022 *Pramana J. Phys.* **96** 192
[13] Wang D S, Zhang D J and Yang J K 2010 *J. Math. Phys.* **51** 023510
[14] Yang J 2019 *Phys. Lett. A* **383** 328
[15] Li Y, Xia Y R, Yao R X and Lou S Y 2026 *Chin. Phys. Lett.* **43** 010002
[16] Zhao L C, Meng L Z, Qin Y H, Yang Z Y and Liu J 2025 *Chin. Phys. Lett.* **42** 110002
[17] Cui X N, Zhang Z Y, Liu M W, Qi F H and Liu W J 2025 *Chin. Phys. Lett.* **42** 100402
[18] Zhao Y, Liu W, Wang L J, Fan Z, Zhou Q, Malomed B A, Chen S F and Xu S L 2025 *Chin. Phys. Lett.* **42** 090002
[19] Escoria J M and Suazo E 2024 *Mathematics* **12** 2694
[20] Zhou G, Luo R and Qi Y 2023 *Phys. Eng.* **33** 79
[21] Serkin V N and Hasegawa A 2000 *Phys. Rev. Lett.* **85** 4502
[22] Shukla P K and Eliasson B 2011 *Rev. Mod. Phys.* **83** 885
[23] Kivshar Y S and Agrawal G P 2003 *Optical Solitons: From Fibers to Photonic Crystals* (Academic Press)
[24] Ablowitz M J and Segur H 1981 *Solitons and the Inverse Scattering Transform* (SIAM)
[25] Skryabin D V and Gorbach A V 2010 *Rev. Mod. Phys.* **82** 1287
[26] Mollenauer L F and Gordon J P 2006 *Solitons in Optical Fibers: Fundamentals and Applications* (Academic Press)
[27] Benjamin T B and Feir J E 1967 *J. Fluid Mech.* **27** 417
[28] Otajonov S R, Umarov B A and Abdullaev F K 2025 *Phys. Scr.* **100** 045403
[29] Sasireka R, Sabari S, Uthayakumar A, *et al.* 2025 arXiv:2509.14831
[30] Liu Y, Xue Y L and Yu C 2015 *Opt. Commun.* **339** 66
[31] Tchepemen N, Tchokouansi H T, Kuetche V K and Bouetou T B 2023 *Nonlinear Dyn.* **111** 20311
[32] Jin G R, Kim C K and Nahm K 2005 *Phys. Rev. A* **72** 045601